Random Semiconductor Lasers: Scattered versus Fabry-Perot Feedback

S. Kalusniak, H. J. Wünsche, and F. Henneberger

Institut für Physik, Humboldt Universität zu Berlin, Newtonstraße 15, 12489 Berlin, Germany

(Received 8 September 2010; revised manuscript received 26 November 2010; published 5 January 2011)

As a result of growth imperfections, (Zn, Cd)O/ZnO quantum well structures exhibit random laser action. Fabrication of microresonators allows us to study and to compare directly cavity and scattered feedback. Our experimental and theoretical analysis shows that (i) pure random lasing generally requires a larger gain than in the standard Fabry-Perot regime, (ii) the presence of Mie scatterers in the semiconductor-based cavity does not substantially increase the lasing threshold, and (iii) the random feedback creates a subtle modal gain distribution that might be of particular importance for the dynamical properties, both with and without Fabry-Perot cavity.

DOI: 10.1103/PhysRevLett.106.013901 PACS numbers: 42.55.Zz, 42.25.Dd, 42.55.Px

Random lasers (RL) have attracted considerable attention during recent years [1]. Here, the feedback for laser action is not provided by an external resonator, but by scatterers which are randomly distributed in an active medium or which by themselves act as optical amplifiers. When aiming at practical applications, random lasing of semiconductor nanostructures is of particular interest. Demonstrations in this area include nanoparticles in powders [2], nanorods [3], and textured quantum well (QW) structures [4]. In this context, the question arises of how the operational parameters (threshold, mode spectrum, directionality) of random lasers compare with those of the standard Fabry-Perot (FP) arrangement, commonly used for semiconductor laser devices today. Imagine that a FP laser cavity is randomly filled with an increasing number of passive scattering centers. The scatterers induce extra losses and, as one might simply conclude, the laser threshold increases. On the other hand, random lasing is expected to emerge when the number and strength of the scatterers exceed certain levels. The interplay between these two processes is the subject of this Letter.

The nanostructures under study are ZnCdO/ZnO QWs which are capable of laser action in a spectral range extending from ultraviolet to green wavelengths [5]. The structures are fabricated by molecular beam epitaxy on sapphire substrates and contain typically 5–10 ZnCdO QWs as active layers. Details about sample preparation and design are found in Ref. [5]. Lasing is generated by optical pumping using 20-ns pulses from a tunable dye-excimer laser system. The samples are excited on their top side along the c axis of the wurtzite crystal structure, while the emission propagating in the plane of the QWs is recorded from the sample edges [see Fig. 1(a)]. The excitation wavelength is 360 nm.

Typical data on the laser action are exemplified in Fig. 1. The excitation is along a stripe of width $w = 300$ μm and variable length $L = 0.3$–3 mm. The stripe is positioned at sufficient distance from the sample edges so that feedback from the semiconductor-air interface is suppressed by absorption in the passive region. Figure 1(b) demonstrates the transition from spectrally broad spontaneous emission to narrow laser action at sufficiently strong pumping. There is a well-defined lasing threshold decreasing down to a few 10 kW/cm^2 for the longest L (inset). The spectrum of lasing modes is shown in Fig. 1(c) under different excitation conditions. There is no correlation between the mode spacing and the length of the sample or the excitation stripe. Excitation with a radially symmetric spot yields qualitatively identical mode spectra at a slightly increased threshold. The number and relative intensity of the modes are very sensitive to the excitation level. Far above threshold, single mode features become less distinctive and an envelope-type spectrum develops (upper panel). For the same reason, averages taken typically over 100 excitation pulses produce apparently smoother mode spectra than single-shot measurements as a result of power fluctuations (center and lower panels). All these findings exclude that the laser action is related to feedback from a FP-type cavity. The key for explaining the observations is found when inspecting the light emerging from the top surface of the sample, i.e., perpendicular to the propagation of the laser emission. Figure 1(d) reveals the existence of discrete scattering centers on a macroscopic length scale with densities of some 100 per mm^2. Examination by scanning electron microscopy (SEM) shows that these scatterers are related to holes in the surface with typical diameters between 0.5 and 1 μm. These holes probably originate from locally impaired nucleation at the sapphire surface when starting the low-temperature growth of the QW structure. We conclude that irregularities of such type do not simply worsen the optical properties as one might naively expect, but give rise to random lasing.

In order to compare random versus FP lasing, microresonators with a natural facet reflectivity of about $R = 0.1$ are fabricated (see Ref. [5]). They are homogeneously excited across their width. Figure 2(a) depicts the lasing threshold of the microresonators as a function of their inverse length along with the same dependence for stripe

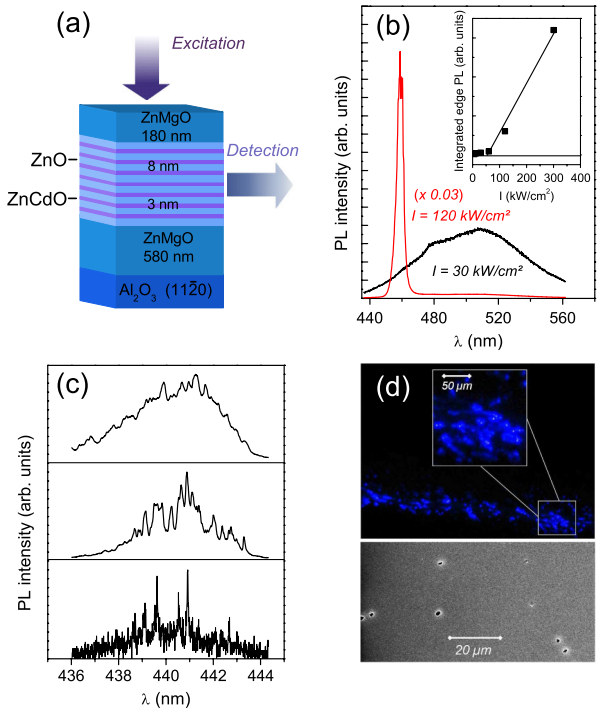

FIG. 1 (color online). Laser action of ZnCdO/ZnO QW structures. (a) Schematics of the samples, not true to scale. (b) Spectral shape of the edge emission at low and high excitation intensity I (7 wells of width $d_w = 3.1$ nm and Cd concentration $x = 0.16$). Inset: Spectrally integrated emission yield versus I. (c) Spectrum of lasing modes ($L = 3$ mm, $d_w = 3.2$ nm, $x = 0.10$). Upper panel: Average spectrum over 100 excitation shots at $I = 300$ kW/cm^2. Center panel: The same at $I = 120$ kW/cm^2. Lower panel: Spectrum under single-shot excitation at $I = 120$ kW/cm^2. (d) Upper panel: Scattered light detected under laser action from the sample surface, i.e., perpendicular to the propagation of the laser emission. Lower panel: SEM image of the sample surface.

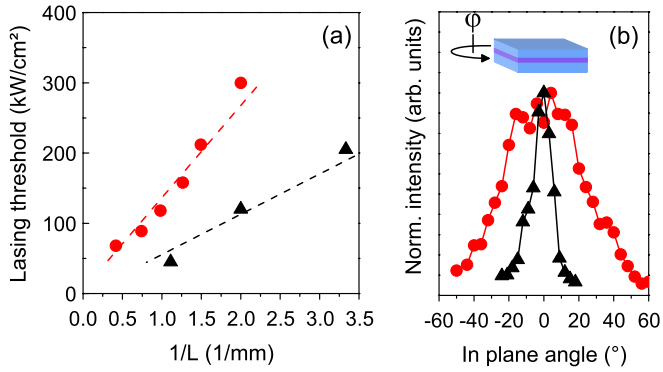

FIG. 2 (color online). Laser action of microresonators (triangles) and unstructured samples (dots). (a) Lasing threshold versus inverse length of the resonator (width of cracked stripe) and of the excitation stripe, respectively. (b) Far-field pattern of the laser emission taken in the plane of the QWs as shown in the inset.

excitation of unstructured samples taken from the same wafer. In both cases, the relation is in good approximation linear; however, the thresholds of the microresonators are about 2–3 times lower. The FP feedback is also manifested in the far-field emission pattern where the beam divergence decreases by about a factor of 5 [Fig. 2(b)]. The fact that the threshold depends on the size of the excitation region excludes that localized modes are predominantly involved in the laser action [6]. Further information is contained in the mode spectra of resonator structures presented in Fig. 3. The FP mode spacing of the $L = 300$ μm resonator is estimated to be $\Delta\lambda = 0.14$ nm. Instead, the average emission spectrum exposes spectral features with roughly 1 order of magnitude larger separation [Fig. 3(a)]. Strikingly, these super modes resolve indeed in sharp peaks with exactly the FP separation in the single-shot excitation regime [Fig. 3(b)]. While the overall appearance of the super modes is very similar for all cavity lengths studied, their number and intensity are again strongly power dependent. Figure 3(c) displays the weakly structured average spectrum of a $L = 900$ μm resonator far above threshold. However, the Fourier decomposition even of such smooth average spectra uncovers clearly a periodicity matching the resonator length [Figs. 3(d) and 3(e)]. These findings indicate a subtle mode organization resulting from the interplay between cavity and random feedback.

Many aspects of light propagation in random media can be adequately treated in terms of point scatterers [7]. For weak scatterers embedded in a host of extension L and gain coefficient g, that pair with the largest separation ($\sim L$) is dominating the laser action and the threshold gain in a two-dimensional setting is easily derived [8],

$$g_{\mathrm{th}}^{\mathrm{RL}} L = \ln(2\pi L/\sigma), \tag{1}$$

where σ denotes the isotropic Rayleigh cross section (with dimension of a length). When compared with the threshold of the standard FP laser $g_{\mathrm{th}}^{\mathrm{FP}} L = \ln(1/R)$, it follows that $g_{\mathrm{th}}^{\mathrm{FP}} \ll g_{\mathrm{th}}^{\mathrm{RL}}$ for typical semiconductor-air reflection coefficients, as per definition $\sigma \ll \lambda \ll L$. In contrast, the threshold increase for the random laser of the present study is only quite modest, indicating scattering markedly stronger than accountable in the Rayleigh limit. The theoretical analysis has thus to be extended to Mie scattering taking into consideration the finite size of the entities. So far, only the case up to six Mie scatterers located in a small μm-sized gain region has been addressed by finite-difference time-domain calculations [8]. The following approach is based on a direct calculation of the complex mode spectrum by solving the nonlinear eigenvalue problem for the scattering amplitudes allowing for a systematic treatment of much larger configurations. We also present a method of how cavity mirrors can be included enabling us to investigate the interplay between random and FP feedback.

In analogy to the experiment, we consider in-plane scattering of transverse waves by N cylindric air-filled holes of radius a randomly distributed in a rectangular stripe with constant gain g, refractive index n, and end reflectivity R [see inset Fig. 4(a)]. The field acting on a

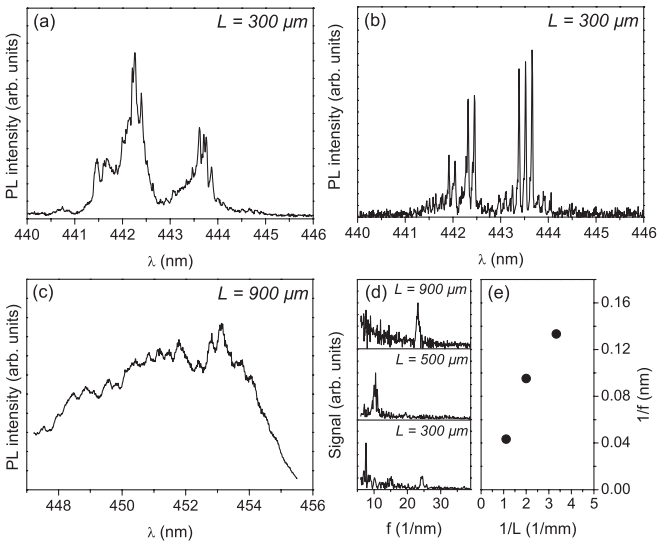

FIG. 3. Mode organization in microresonator structures ($d_w = 3.1$ nm, $x = 0.16$). (a) Average mode spectrum of a $L = 300$ μm resonator ($I = 250$ kW/cm^2). (b) The same taken for 5 excitation shots only. (c) Average mode spectrum of a $L = 900$ μm resonator ($I = 620$ kW/cm^2). (d) Fourier decomposition of envelope-type average spectra well above threshold for different resonator lengths, upper plot is gained from (c). (e) Mode separation $\Delta\lambda$ deduced from (d) versus inverse resonator length.

particular scatterer s at planar position $\vec{r}_s = (x_s, y_s)$ is the superposition of partial fields outgoing from all other scatterers at positions $\vec{r}_{\bar{s}}$ and from the mirrors at $x_m = mL/2$ with $m = \pm$. The distances r_{sq} between the scatterers ($q = \bar{s}$) as well as between the scatterers and the mirrors ($q = m$) obey $r_{sq} \gg \lambda, a$. Hence, the partial fields incident from q on s can be approximated by transverse plane waves with scalar amplitudes E_{sq} and propagation unit vectors $\vec{n}_{sq}$, as in the standard case of external light scattering [9]. This yields a system of $N(N+1)$ linear homogeneous equations [10]:

$$E_{sq} = \sum_{\bar{s},\bar{q}}^{\bar{q}\neq\bar{s}} S_{sq,\bar{s}\,\bar{q}} E_{\bar{s}\,\bar{q}},$$

$$S_{sq,\bar{s}\,\bar{q}} = \begin{cases} G(k, r_{sq}) A(\vec{n}_{sq}\vec{n}_{\bar{s}\,\bar{q}})\delta_{q\bar{s}} & (q \in \text{scatterers}) \\ Q_{sq,\bar{s}\,\bar{q}} & (q \in \text{mirrors}). \end{cases} \quad (2)$$

The upper line stands for direct coupling between $\bar{s}$ and s, while reflection on a mirror before the field from $\bar{s}$ arrives at s is accounted for in the lower line. $A(\vec{n}_{\text{out}}\vec{n}_{\text{in}})$ represents the angle-dependent plane-wave scattering amplitude taken for a cylinder with both polarization as well as propagation direction of incoming and outgoing field perpendicular to its axis [9]. The far-field Green function $G(k, r) = \exp(ikr + i\pi/4)/\sqrt{8\pi kr}$ of the two-dimensional Helmholtz equation describes the propagation of the outgoing wave in the gain region with wave number $k = k_0 - ig/2$. Inclusion of the mirror feedback is not straightforward as the scatterers couple on and off cavity axis propagating light yielding unlimited amplification in an infinite transverse geometry. We make use of the waveguide character of a gain region with finite transverse width w. Expanding scattered waves in series of the waveguide modes ν solving $[\nabla_y^2 + k^2(y)]\phi_\nu(y) = \beta_\nu\phi_\nu(y)$ under radiating boundary conditions yields [10]

$$Q_{sm,\bar{s}\,\bar{q}} = \frac{\sqrt{R}}{2ik}\sum_\nu \phi_\nu(y_s)\phi_\nu(y_{\bar{s}})e^{i\beta_\nu r_{sm}} \times \frac{A(\vec{n}_{m\bar{s}}\vec{n}_{\bar{s}\,\bar{q}})e^{i\beta_\nu r_{m\bar{s}}} - A(\vec{n}_{-m\bar{s}}\vec{n}_{\bar{s}\,\bar{q}})\sqrt{R}e^{i\beta_\nu(L+r_{-m\bar{s}})}}{1 - Re^{2i\beta_\nu L}}. \quad (3)$$

Already, accounting for the fundamental mode has provided sufficient precision in the calculations presented below. Solving $\det[\delta_{s\bar{s}}\delta_{q\bar{q}} - S_{sq,\bar{s}\,\bar{q}}(k)] = 0$ for complex k provides the spectral position of the lasing modes (real part) as well as their threshold gain g_{th} (imaginary part).

In the numerical analysis, the positions of the scatterers within the gain region are set by a random number

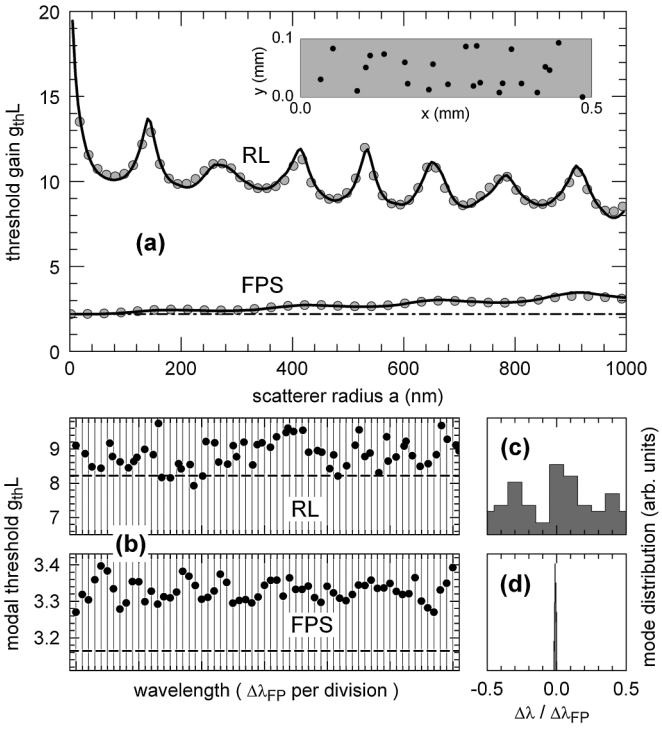

FIG. 4. Laser action of randomly distributed Mie scatterers for a semiconductor-hole system. RL, scatterers only ($R = 0$); FPS, scatterers with FP cavity. (a) Threshold gain $g_{\text{th}}L$ versus scatterer radius a. Inset: Position of the scatterers within the gain stripe. Black solid line: Full solution of Eqs. (2) and (3). Circles: Weak-scattering approximations (see text). Dash-dotted line: $\ln(1/R)$. (b) Modal thresholds versus spectral position ($a = 480$ nm). Note enlarged vertical scale. Dashed horizontal lines: $g_{\text{th}}L$ from (1) with σ_b and (4), respectively. Vertical lines: Mode positions λ_{FP} of the pure FP laser. (c),(d) Corresponding distribution of deviations from λ_{FP}. Parameters: $N = 24$, $c = v_g = c_0/n$, $n = 2$, $L = 500$ μm, $w = 100$ μm, mirror reflectivity $R = 0.11$.

generator. Unrealistic configurations, where, e.g., $r_{s\bar{s}} \lesssim \lambda$, are disregarded. Searching for the some-10 modes of lowest g_{th} within a few nm wide spectral interval around center wavelength $\lambda = 500$ nm is sufficient to obtain representative results. While detailed position and threshold gain depend on the specific configuration under study, there are a number of general features that are commonly found in all calculations. Figure 4 summarizes such features computed for parameters of the ZnCdO/ZnO QW structures.

Black solid curves in Fig. 4(a) represent the threshold gain as a function of the scatterer radius a. In the Rayleigh limit $a \ll \lambda$, as already argued above, the threshold of the pure random laser with no mirrors is much larger than that of the untainted FP laser (dash-dotted line). Consistently, the threshold of the FP with scatterers (FPS) is here practically identical with $\ln(1/R)$. An initially distinct lowering of the RL threshold for increasing radius devolves into a plateaulike behavior when $a \gtrsim \lambda/n$. For the FPS, there is merely a slight threshold increase. Both curves are superimposed by modulations caused by interference effects, which becomes clear in what follows.

Interestingly, though a becomes significantly larger than λ/n, the scattering is still weak in the sense that couplings involving more than pairs of scatterers can be neglected. In this case, approximation formulas for the threshold gain can be analytically derived [10]. Indeed, these approximations (circles) reproduce very well the full numerical curves. The weak-scattering RL threshold reads as formula (1), but with the isotropic σ replaced by the Mie backscattering cross section $\sigma_b = |A_\pi|^2/(4k_0)$ [8]. The threshold modulations are due to resonances of this cross section. Maxima occur when waves reflected at the front and back side of the scatterer interfere destructively, i.e., approximately at radii being integer multiples of $\lambda/2$. The approximation for the FPS is [10]

$$g_{\mathrm{th}}^{\mathrm{FPS}} L = \ln(1/R) + N\sigma_{\mathrm{ext}}/w, \tag{4}$$

where $\sigma_{\mathrm{ext}} = \mathrm{Im}A_0/k_0$ is the Mie extinction cross section. The correction to the pure FP term is due to forward scattering of the wave circulating in the cavity. Each scatterer casts a shadow of size σ_{ext}. The extinction cross section of a large object is twice its geometrical cross section so that $g_{\mathrm{th}}^{\mathrm{FPS}}$ is an increasing function of a. The weak modulations are due to interference between waves crossing and bypassing the scatterer.

The difference in the thresholds of RL and FPS agrees reasonably well with the experimental data in the relevant scatterer size range. Waveguide losses in the vertical direction can thus not play an essential role. Fluctuations of the scatterer size average out the modulations predicted theoretically. The right-hand side of formula (1) is only a very smooth function of the stripe length, explaining why the threshold of both RL and FPS follow closely a $1/L$ dependence in the experiment.

Figure 4(b) depicts the modal threshold gain versus spectral mode position ($a = 480$ nm). As $g = \mathrm{const}$, all modes were exhibiting the same threshold in the pure FP and variations are thus a consequence of random feedback. Unlike steady state, a large number of modes contribute to the time-integrated emission under pulsed excitation. However, those with the lowest threshold are dominant and form the supermodes observed in the experiment, both for unstructured and microresonator samples. While the RL threshold gain can be well estimated by two scatterers at distance L, the presence of other scatterers leads to significant fluctuations of the spectral mode spacing [Fig. 4(c)]. In contrast, the FPS modes are practically pinned to the positions of the pure FP cavity, again fully consistent with the measurements [Figs. 3(d) and 4(d)].

In summary, our above study has revealed various aspects of random feedback in semiconductor nanostructures. First, pure random lasing typically requires a larger gain than under FP feedback, even if only the relatively small natural facet reflectivity is utilized. Obviously, ZnO-based structures are predestined in this regard because of their large excitonic gain. Second, as long as $N\sigma_{\mathrm{ext}}/w < \ln R$, the presence of scatterers does not substantially deteriorate the overall lasing threshold of a FP cavity. However, third, the random feedback creates a subtle modal gain distribution that might be of particular importance for the dynamical properties, both with and without cavity.

This work was supported by DFG in the frame of Sfb 555. The authors thank Sergey Sadofev for growing the QW structures and Simon Halm for helpful discussions.

[1] Reviews about random lasers are found in H. Cao, J. Phys. A **38**, 10 497 (2005); D. S. Wiersma, Nature Phys. **4**, 359 (2008); O. Zaitsev and L. Deych, J. Opt. **12**, 024001 (2010).

[2] H. Cao *et al.*, Phys. Rev. Lett. **82**, 2278 (1999); M. A. Noginov *et al.*, Laser Phys. Lett. **1**, 291 (2004); J. Fallert *et al.*, Nat. Photon. **3**, 279 (2009).

[3] S. F. Yu *et al.*, Appl. Phys. Lett. **84**, 3241 (2004); H. Y. Yang *et al.*, Appl. Phys. Lett. **89**, 081107 (2006).

[4] S. Chu *et al.*, Appl. Phys. Lett. **93**, 181106 (2008); H. K. Liang, S. F. Yu, and H. Y. Yang, Appl. Phys. Lett. **96**, 101116 (2010).

[5] S. Kalusniak *et al.*, Laser Photon. Rev. **3**, 233 (2009).

[6] V. M. Apalkov, M. E. Raikh, and B. Shapiro, Phys. Rev. Lett. **89**, 016802 (2002).

[7] See, for example, M. C. W. van Rossum and Th. M. Nieuwenhuizen, Rev. Mod. Phys. **71**, 313 (1999).

[8] X. Wu *et al.*, Phys. Rev. A **74**, 053812 (2006).

[9] Craig F. Bohren and Donald R. Huffman, *Absorption and Scattering of Light by Small Particles* (Wiley-VCH, Weinheim, 2004).

[10] See supplementary material at http://link.aps.org/supplemental/10.1103/PhysRevLett.106.013901 for details of the derivation.